JOURNAL OF PROPULSION AND POWER
Vol 8, No. 2, March–April 1992

Three-Dimensional Viscous Analysis of a Mach 5 Inlet and Comparison with Experimental Data

D. R. Reddy*
Sverdrup Technology, Inc., Lewis Research Center Group, Brook Park, Ohio 44142
and
L. J. Weir†
NASA Lewis Research Center, Cleveland, Ohio 44135

A time-marching three-dimensional full Navier-Stokes code is applied to simulate the flow for a Mach 5 inlet experimental configuration using the data obtained in the 10- × 10-ft supersonic wind tunnel at the NASA Lewis Research Center. For the first time, a solution is obtained for this configuration with the actual geometry, the tunnel conditions, and all the bleed zones modeled in the computation. Computed pitot pressure profiles and static pressures at various locations in the inlet are compared with the corresponding experimental data. The effect of bleed zones is simulated reasonably well using approximations for the bleed boundary conditions and the turbulence model.

Introduction

THE flow through a hypersonic inlet is characterized by complex three-dimensional flow phenomena such as strong secondary flows and shock/boundary-layer interactions. Since these phenomena can have significant effect on the overall performance of the inlet, any numerical method used to simulate the flow through the inlet must be capable of accurately predicting these complex phenomena. Therefore it is essential that a code selected for computing the inlet flows be thoroughly validated with experimental data to verify its capability to simulate correctly the above mentioned flow features. The objective of this study is to assess the capability of the numerical code using the data obtained from an experimental study of a Mach 5 inlet conducted at the NASA Lewis Research Center 10- × 10-ft supersonic wind tunnel facility.

A full Navier-Stokes time-marching code, PARC3D,[1] was selected for the inlet flow computations. The PARC3D code solves the full three-dimensional Reynolds-averaged Navier-Stokes equations in strong conservation form with the Beam and Warming approximate factorization. The code was originally developed as AIR3D by Pulliam and Steger,[2] and Pulliam[3] later added the Jameson[4] artificial dissipation and called the code ARC3D. Cooper[1] adapted the code for internal flow in propulsion applications and named the code PARC3D. The PARC3D code uses central differencing on a generalized curvilinear coordinate system with implicit and explicit second- and fourth-order artificial dissipation. To simplify the solution of the block pentadiagonal system of discretized equations, the block implicit operators are diagonalized by decomposing the flux Jacobians resulting in a scalar pentadiagonal system. The loss of time accuracy due to the diagonalization does not affect the spatial accuracy of the steady-state solution.[3] The turbulence model used in the code for this study is the Baldwin-Lomax model.

The PARC3D code has been verified previously for three-dimensional supersonic and two-dimensional hypersonic flow configurations[5] with flow features similar to those of hypersonic inlets. These studies demonstrated the capability of PARC3D to simulate the hypersonic inlet flow phenomena. There was an attempt to compute the flow through a hypersonic inlet model, Generic Option 2 Mach 12.25 model, which was experimentally tested by McDonnell-Douglas at the Calspan test facility.[6] The experimental data indicated that there was turbulent transition in the corner regions of the inlet while the bulk of the flow through the inlet remained laminar. Since the turbulence model in the code does not have the capability to simulate three-dimensional transition, it was not possible to obtain a solution that corresponded to the actual experimental conditions. In the experimental setup of the present study, the incoming flow was tripped by means of a grit (No. 80 size) to make the flow completely turbulent before it entered the inlet and it remained turbulent through the entire inlet.

The Mach 5 inlet configuration has been previously analyzed by Benson,[7] Kim et al.[8] using a parabolized Navier-Stokes (PNS) method, and Rose[9] using MacCormack algorithm. However, none of these computations simulated the actual experimental configuration in terms of the flow conditions and the inlet geometry. Benson's computations assumed the inlet Mach number to be 5.0 and did not contain any bleed, whereas the actual inlet has extensive bleed regions on the side walls as well as ramp and cowl surfaces. In addition, the Mach number of the flow at the entrance to the inlet in the wind tunnel was 3.5 with the inlet set up at a negative angle of attack of 8.5 deg so that the flow goes through an expansion at the entrance to a Mach number of 4.1 which is approximately equal to that corresponding to a flight Mach number of 5 with a 9-deg angle of attack (see the following experimental configuration). Kim also assumed an entrance Mach number of 5 and computed the flow with only ramp and cowl bleed. Rose's configuration used side walls beginning from the first ramp instead of the full sidewalls that extend all the way to the leading edge of the precompression ramp (Fig. 1). Moreover, only the sidewall bleed close to the cowl surface was considered in his computations.

Presented as Paper 90-0600 at the AIAA 28th Aerospace Sciences Meeting, Reno, NV, Jan. 8–11, 1990; received Nov. 19, 1990; revision received March 15, 1991; accepted for publication March 18, 1991.

*Present address: Chief, Computational Fluid Dynamics Branch, NASA Lewis Research Center, M.S. 5-11, 21000 Brookpark Road, Cleveland, OH 44135. Member AIAA.
†Aerospace Engineer, M.S. 86-7. Member AIAA.

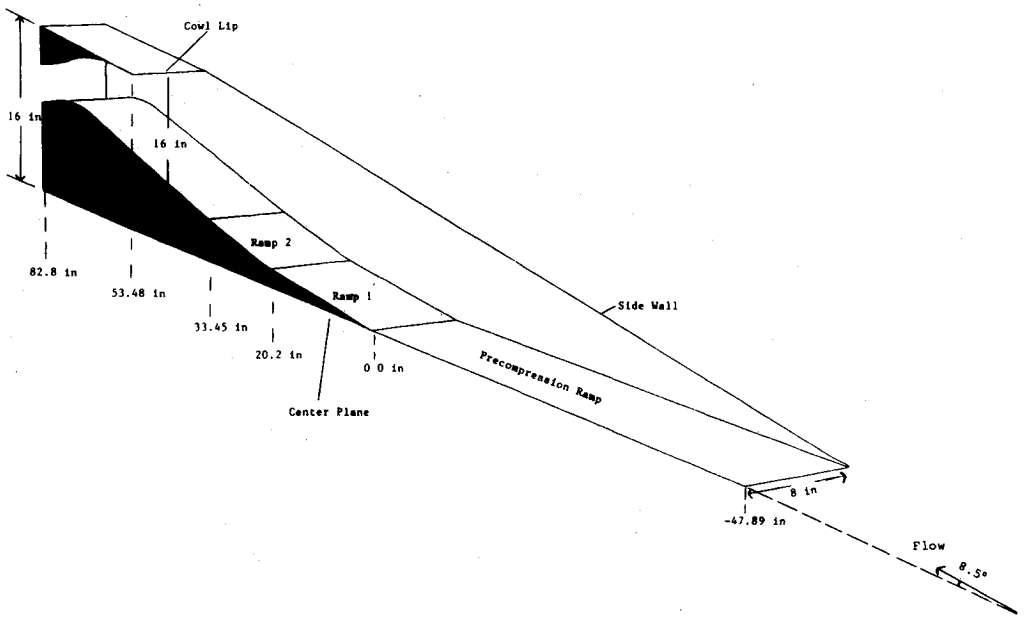

Fig. 1 Inlet model configuration.

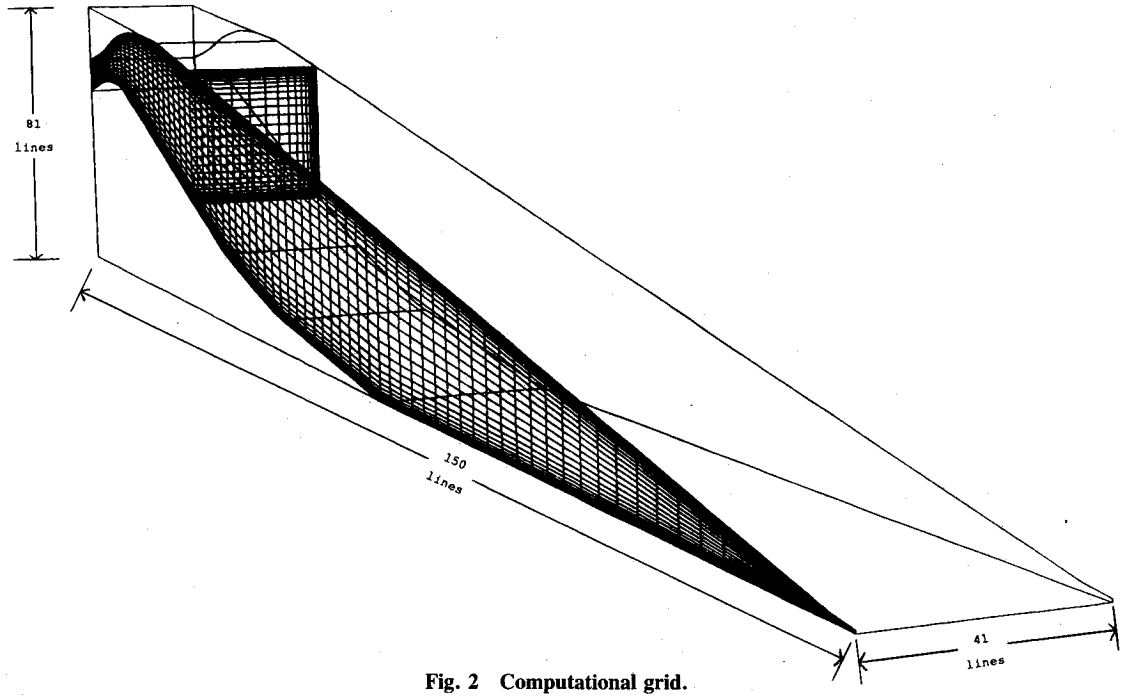

Fig. 2 Computational grid.

In the present study all the bleed regions are simulated in the computation with the actual flow conditions and the geometry used in the wind tunnel.

Experimental Configuration

The experimental inlet is a one-third scale of a proposed Mach 5 aircraft mixed-compression inlet. The configuration is shown in Fig. 1. Since the maximum Mach number that can be obtained in the 10- × 10-ft supersonic wind tunnel at NASA Lewis is 3.5, the inlet is installed at a negative angle of attack of 8.5 deg so that the flow entering the inlet goes through an expansion on the precompression ramp to a Mach number of about 4.1. This simulates a freestream flight Mach number of 5.0 at a 9-deg angle of attack. The Mach number of the flow entering the inlet in the experiment was 3.49 and the tunnel total pressure was 35.1 psi. The Reynolds number based on the tunnel conditions and the cowl height (16 in.) was 3.3 million. A series of wedges (ramps) generate oblique shock waves external to the cowl. The cowl generates an oblique shock inside the inlet which reflects from the ramp surface and terminates in a normal shock downstream of the inlet throat. A subsonic diffuser compresses the flow further. The computations in this study are performed to model only the supersonic flow upstream of the terminal normal shock.

To control shock/boundary-layer interaction through the inlet, boundary-layer bleed is provided on the inlet walls. A number of bleeds are set up in the throat region to obtain data with various bleed combinations. The original purpose of the test was to determine the minimum amount of bleed needed to keep the inlet started. The data obtained includes static pressures and pitot pressure distributions on the ramp, cowl, and sidewall surfaces and in the corner regions at various axial locations through the inlet. Complete details of the experimental setup and the data can be found in Ref. 10.

Computations

The computations are performed on the Numerical Aerodynamic Simulation's Cray-2 computer located at NASA Ames Research Center using a grid size of 150 × 81 × 41. The computational grid showing one each of the streamwise and

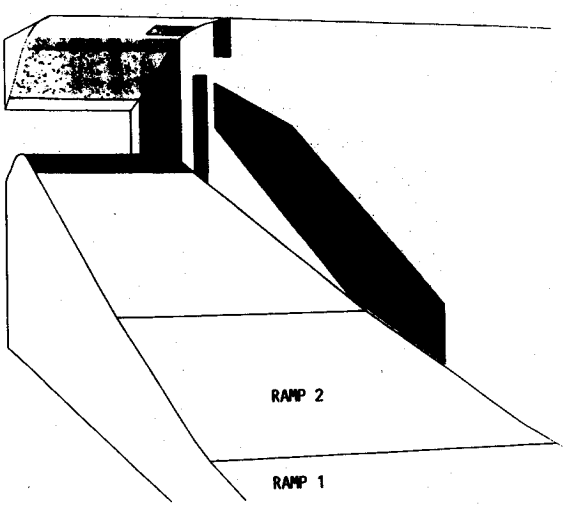

a) Schematic of bleed zones

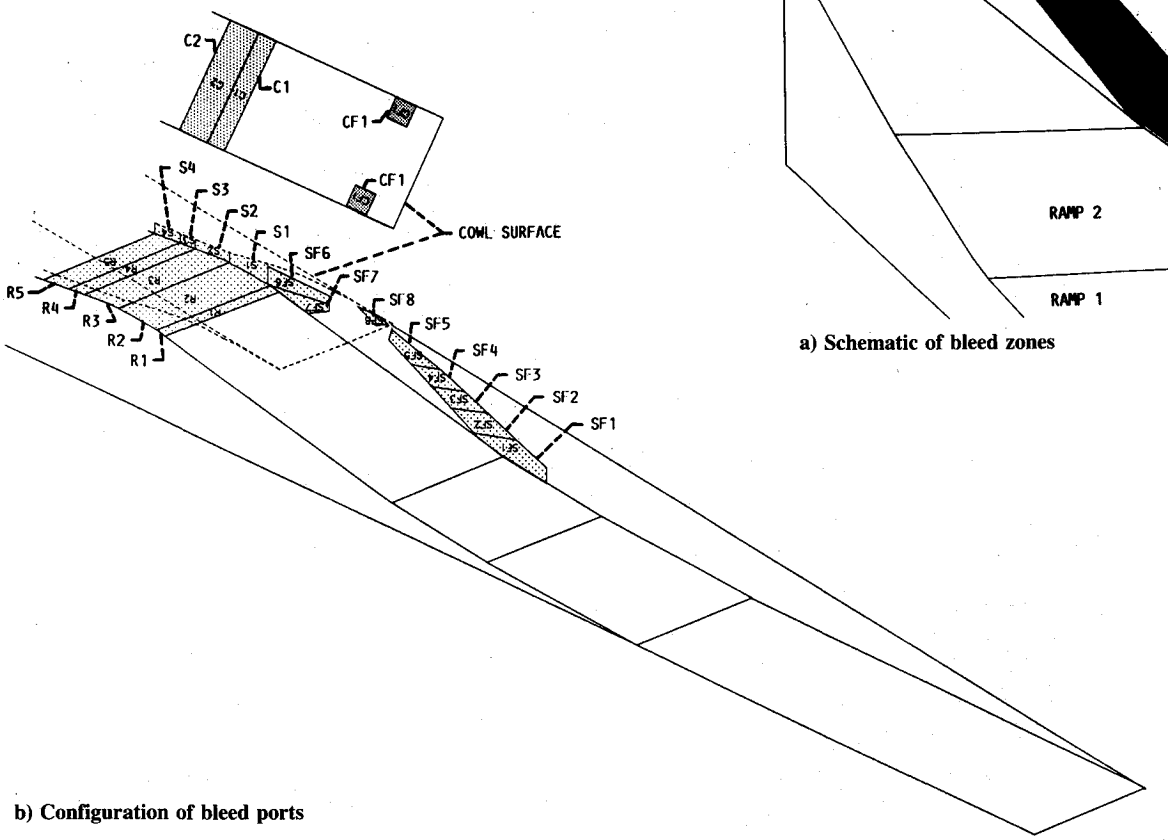

b) Configuration of bleed ports

Fig. 3 Bleed zones.

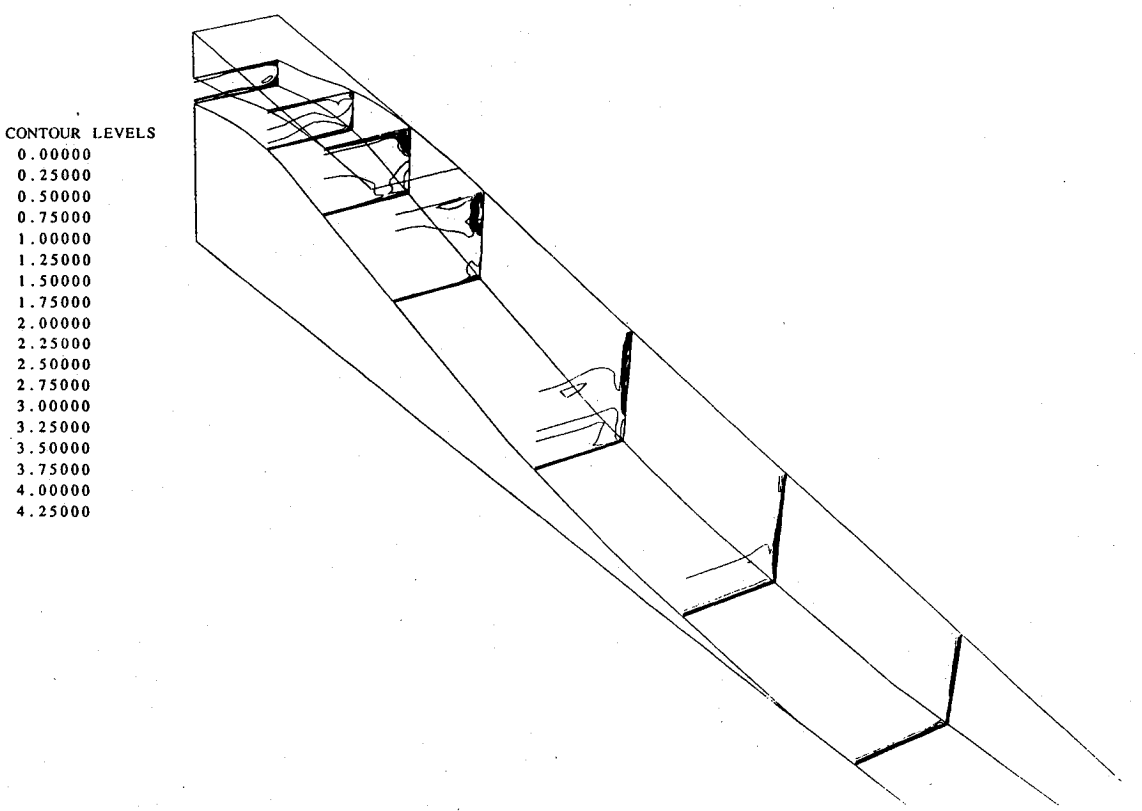

Fig. 4 Mach number contours.

Table 1 Mass flow through bleed ports

Bleed port number	Mass flow through bleed port (mass flow bled/inlet mass flow)
SF1	0.0017
SF2	0.0015
SF3	0.0018
SF4	0.0015
SF5	0.0017
SF6	0.0006
SF7	0.0027
SF8	0.0005
S1	0.0097
S2	0.0110
S3	0.0067
S4	0.005
R1	0.0055
R2	0.0259
R3	0.0326
R4	0.0104
R5	0.0088
CF1	0.0033
C1	0.0225
C2	0.0132

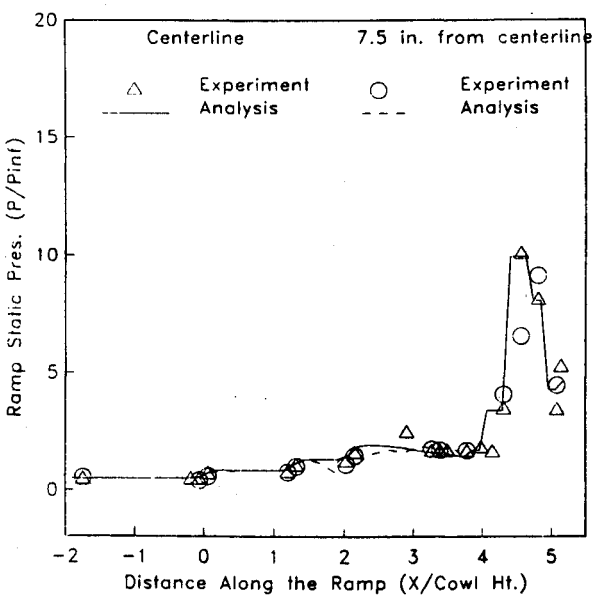

Fig. 5 Ramp static pressure distribution.

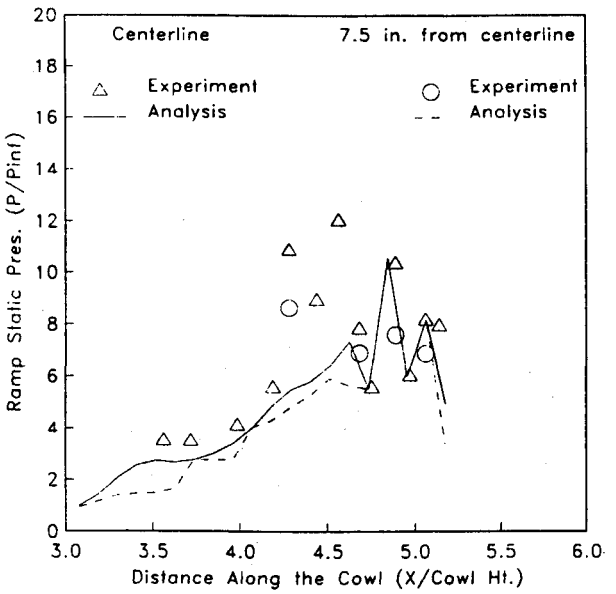

Fig. 6 Cowl static pressure distribution.

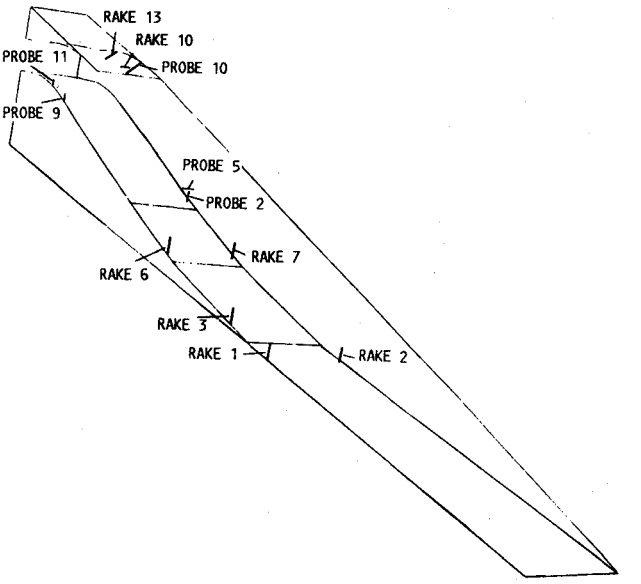

Fig. 7 Location of fixed rakes and translating probes used for pitot pressure measurement.

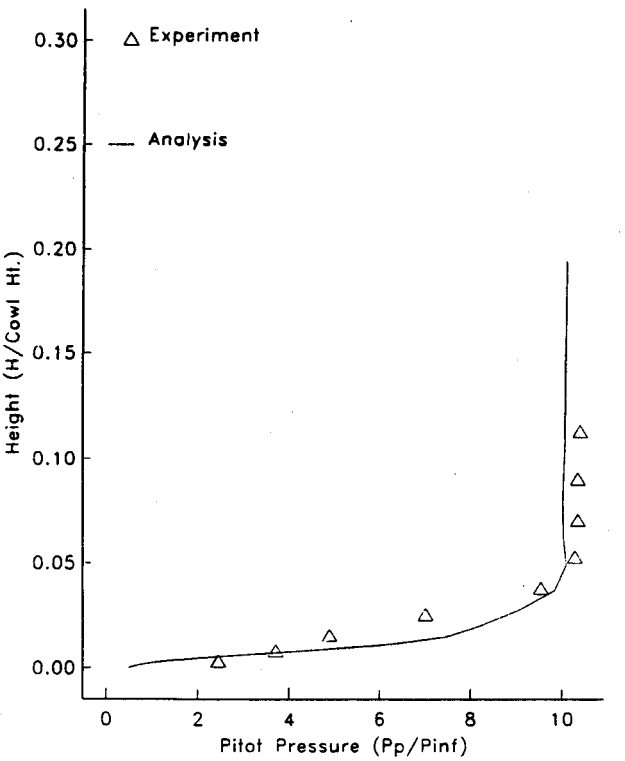

Fig. 8 Rake 1 pitot pressure profile.

transverse planes is shown in Fig. 2. To resolve the viscous layers, the grid lines are clustered in regions close to the walls using hyperbolic tangent functions such that the first grid line away from the wall is located at a y^+ of approximately 2.0. As shown in Fig. 2, the grid lines in the streamwise direction are arranged in such a way that the uppermost grid line follows the edge of the sidewall which joins the leading edge of the inlet ramp with the inlet cowl on each side of the inlet. This is done to facilitate the application of boundary conditions along the sidewall edges.

The run time and memory requirements for one computation are of the order of 20 h and 16 million words, respectively. Since the inlet is symmetric in the transverse (Z) direction, only half of the inlet flowfield is computed with a symmetry condition imposed on the center plane. A nonreflective boundary condition, using a simple Mach wave ex-

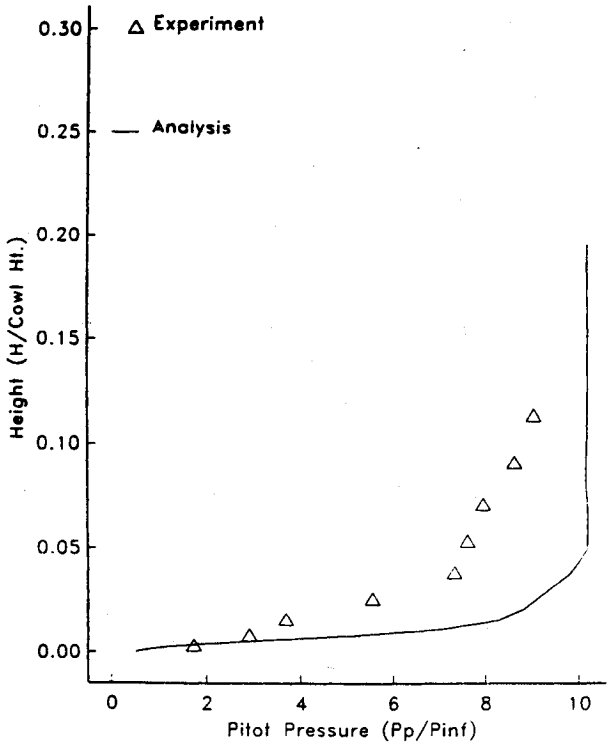

Fig. 9 Rake 2 pitot pressure profile.

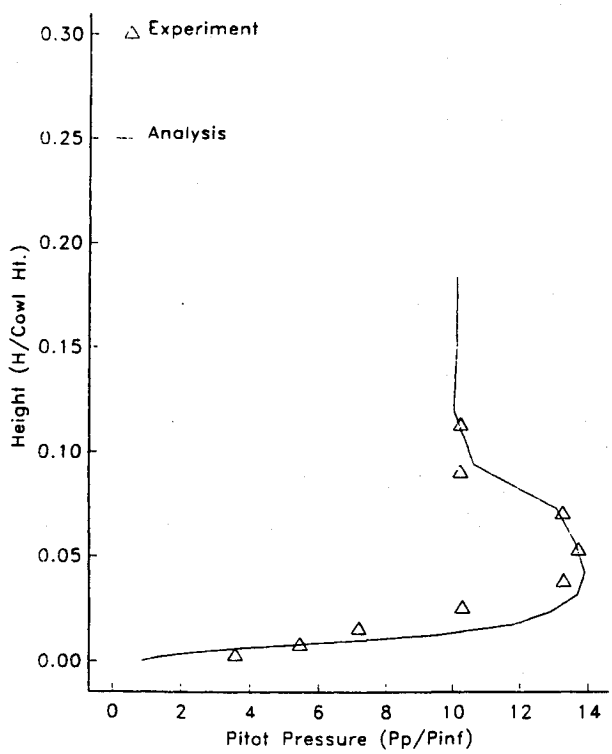

Fig. 10 Rake 3 pitot pressure profile.

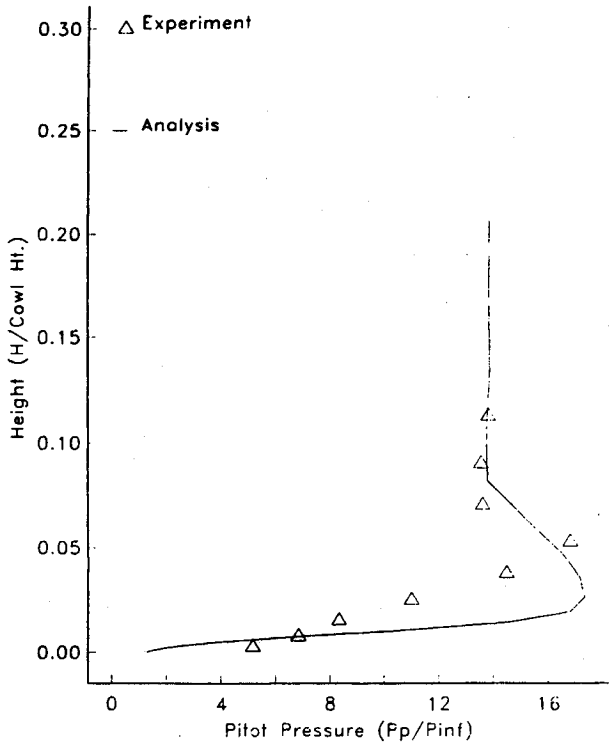

Fig. 11 Rake 6 pitot pressure profile.

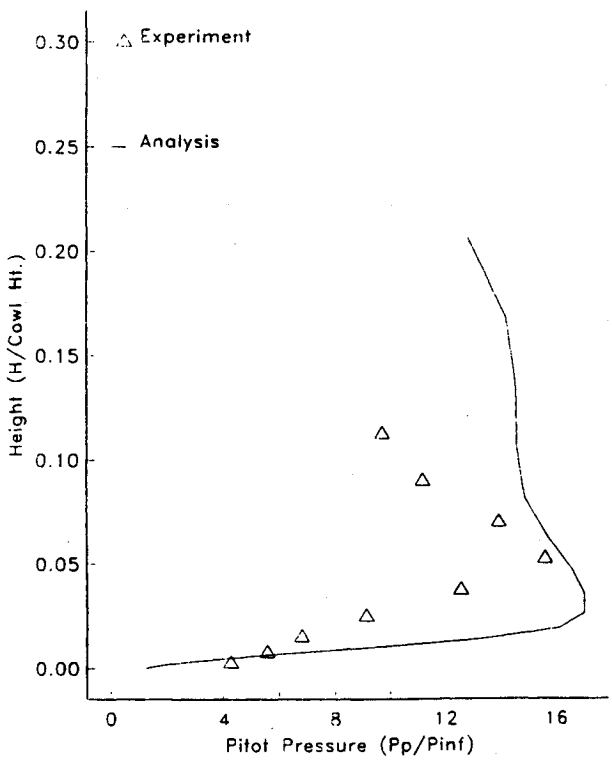

Fig. 12 Rake 7 pitot pressure profile.

trapolation, is applied on the upper boundary upstream of the cowl in order to let the shock waves from the first and second ramps to pass through that boundary. At the inflow boundary, which is ahead of the precompression ramp leading edge, the uniform flowfield is held fixed. At the outflow boundary, the flow variables are extrapolated from inside. No-slip and adiabatic wall conditions are applied on all the solid walls.

Bleed is simulated in the computations by imposing a constant mass flow through each bleed surface: The bleed surfaces are porous with effective bleed area as 40% of the actual area. The mass flow through the bleed regions has been obtained from the experimental data which is determined from the choked condition using the measured plenum and exit pressures for each bleed port. Each bleed port is separately connected to a plenum and the flow through the exit of the plenum is choked by means of a conical plug. The amount of mass flow bled through each bleed port, expressed as a fraction of the incoming mass flow, is given in Table 1. The location of the various bleed zones and their nomenclature used in the

experiment[10] are shown in Figs. 3a and 3b. Numerically the bleed mass flow is uniformly distributed over the surface of each bleed port.

Results and Discussion

The present computations are performed with the bleed boundary conditions applied on all the surfaces corresponding to the various bleed zones. The solution is obtained for the flow conditions identical to those of the experiment with all the bleed ports open.

Figure 4 shows the Mach number contours in the cross planes at selected axial locations. The figure shows shock waves from the different ramp surfaces and the cowl as horizontal lines, and the interaction of the shocks with the boundary layer on the sidewalls. The strong secondary flow set up by this shock/boundary-layer interaction and the migration of the low-energy fluid toward the center plane of the inlet as the flow approaches the throat region can be inferred qualitatively from the contours in Fig. 4. It is the presence of this low-energy fluid occupying a significant portion of the inlet cross-sectional area that degrades the performance of the inlet. The bleed removes this low-energy fluid from the inlet and thereby improves the total pressure recovery. As the flow approaches the throat region that contains bleed, the undesirable low-energy fluid is reduced considerably (Fig. 4). This phenomenon has been substantiated by the experimental data of the two corner rakes which is discussed later.

By examining the location of various bleed ports, shown in Fig. 3, it can be seen that a combination of the first cowl bleed, the sidewall bleed underneath the first cowl bleed, and the downstream cowl bleed appears to be responsible for the elimination of the low-energy vortical fluid. This region is shown in more detail in the pitot pressure contours along with the bleed zones and discussed later in this section.

It should be pointed out here that previous calculations by Rose[9] have indicated that the corner bleed regions do not remove this vortical flow. It can be see from Figs. 3 and 4 that the sidewall bleed located upstream of the cowl seems to have little effect in eliminating this low-energy fluid. This fact has also been observed in experiments by Barnhart[11] and computations by Gaitonde[12] of glancing shock/sidewall boundary interactions. It could be argued that the downstream throat bleed would not have a major influence on the predominantly supersonic flow in the corner region.

Static pressures on the ramp surface both along the centerline and 7.5 in. from the centerline are compared to the corresponding experimental data in Fig. 5. The static pressures and the pitot pressures in all of the comparisons are nondimensionalized with the tunnel static pressure (0.467 psi); the lengths are normalized with cowl height (16 in.). The agreement of the solution with the data is very good throughout the computational length of the inlet. Figure 6 shows a similar comparison for the cowl surface and once again the agreement between the data and the solution is good except in the initial portion where the disagreement is with three of the data points on the centerline and one point at 7.5 in. from the centerline. It has been found that one of the translating probe assemblies is located in the same region where these four static pressure taps are located. The probe assemblies used in the experiment do not completely retract into the walls of the inlet. They project about $\frac{1}{8}$ in. into the flow. Because shock waves are generated from this projection, the data obtained from these four static pressure taps, where the solution disagrees with the data, are not accurate. The disturbance in the flowfield created by the projection is a localized phenomenon that did not affect the flowfield further downstream. Since the four static pressure taps mentioned above happened to be located right in this disturbance, only these four data points are believed to be in error. As can be seen from the rest of the comparison on the cowl surface and on the ramp surface, none of the remaining data points was affected.

Pitot pressure profiles are compared at various locations on the ramp, cowl, and sidewall surfaces. To determine the ability of the bleed ports to bleed the low-energy vortical fluid out of the inlet, two rakes are mounted in the corner of cowl and sidewall surfaces at a 45-deg angle in the throat region. A number of translating probes were also used to measure pitot pressure profiles at various locations on the ramp and sidewall surfaces.

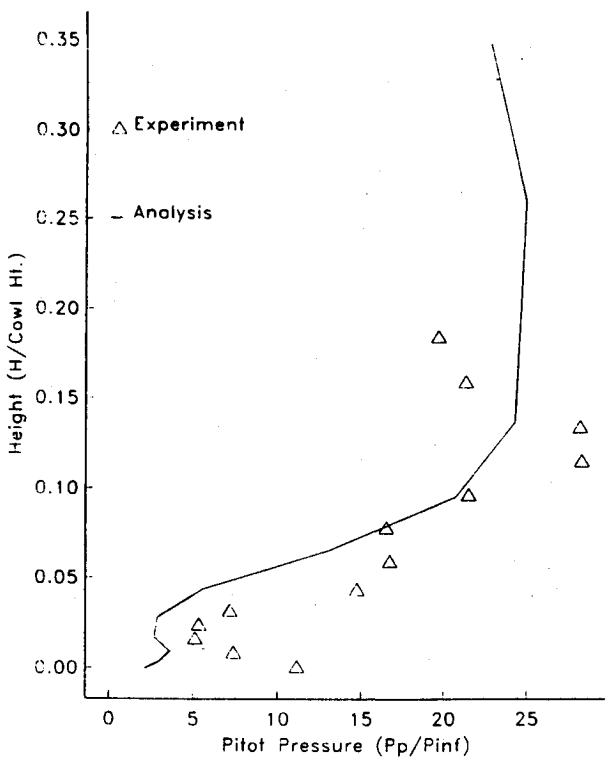

Fig. 13 Rake 10 pitot pressure profile.

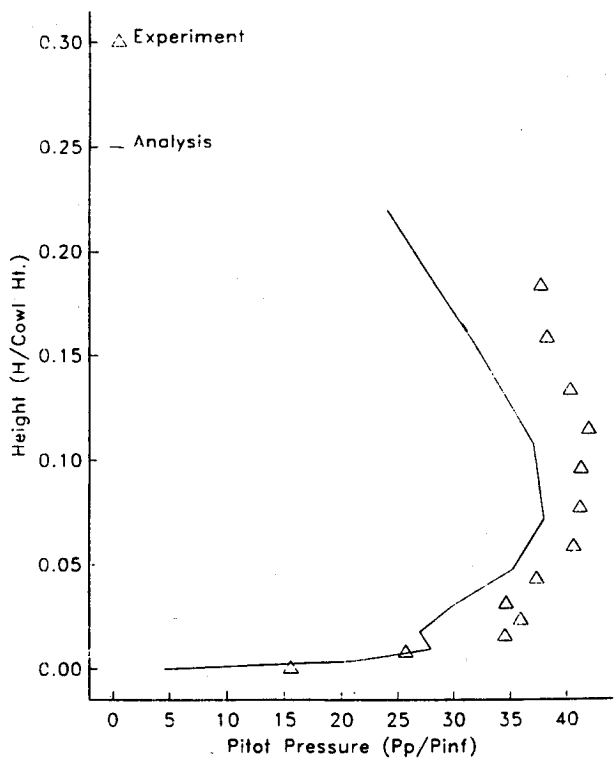

Fig. 14 Rake 13 pitot pressure profile.

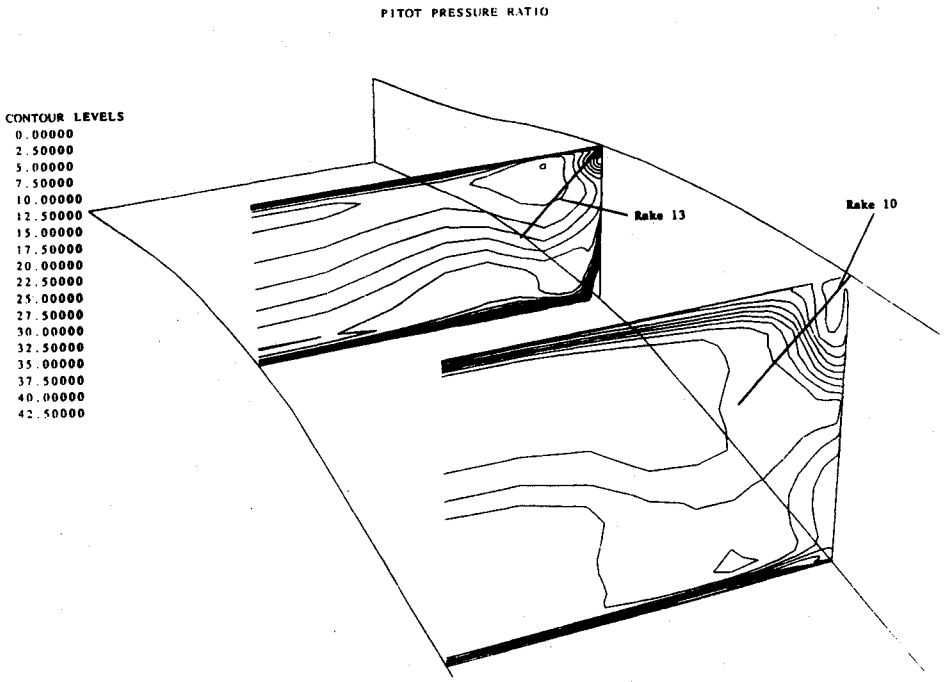

a) At rake 10 and rake 13

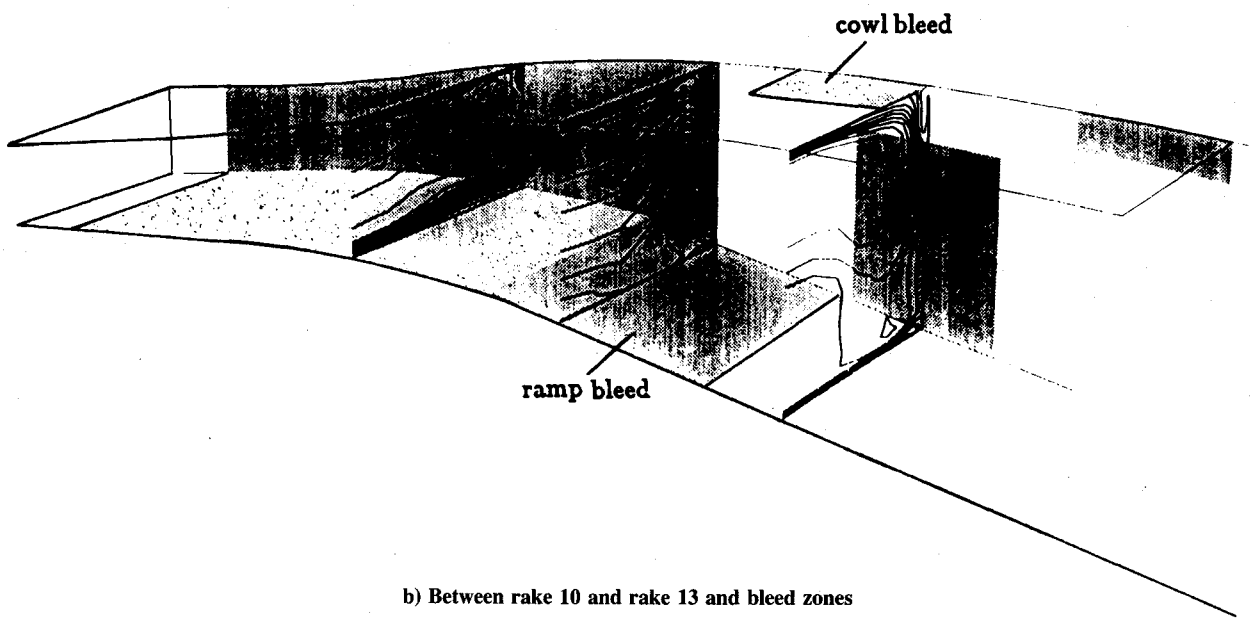

b) Between rake 10 and rake 13 and bleed zones

Fig. 15 Pitot pressure contours.

Since it is not possible to present the comparison of the solution with the data from all of the rakes and probes, only a few rakes and probes that are placed in each of the important regions of the inlet flowfield have been selected. The rake and probe numbers and their locations for which the solution is compared are shown in Fig. 7.

Figures 8 to 12 compare the solution with the experimental data corresponding to pitot pressure rakes located on the ramp surface both along the centerline and close to the sidewall at various streamwise stations. These comparisons show that in general the agreement between the solution and the experimental data is reasonably good along the centerline (rakes 1, 3, and 6). Close to the sidewall the agreement is not so good (rakes 2 and 7). This can be attributed to the corner effect that could not be adequately simulated with the present eddy viscosity turbulence model. A better turbulence model is believed to improve the comparison in the corner regions.

Figures 13 and 14 show pitot pressure comparisons corresponding to rakes 10 and 13, respectively. These rakes are mounted from the corner of cowl and sidewall surfaces at a 45-deg angle to the surfaces. Rake 10 is located at 59.6 in. and rake 13 is located at 68.5 in. from the start of ramp 1 (Figs. 1 and 7). As mentioned earlier, most of the low-energy vortical flow is removed from the inlet between these two rakes. The profile of rake 10 shows great variations in the pitot pressure as we move along the rake away from the corner, whereas that of rake 13 (Fig. 14) shows that the variation has greatly reduced.

This variation in the pitot pressure due to the presence of the vortical flow can also be seen qualitatively in the pitot pressure contours in Figs. 15a and 15b. Figure 15a shows the computed pitot pressure contours for the two cross sections corresponding to rake 10 and rake 13, along with the rake locations in the cross sections. Figure 15b also shows the

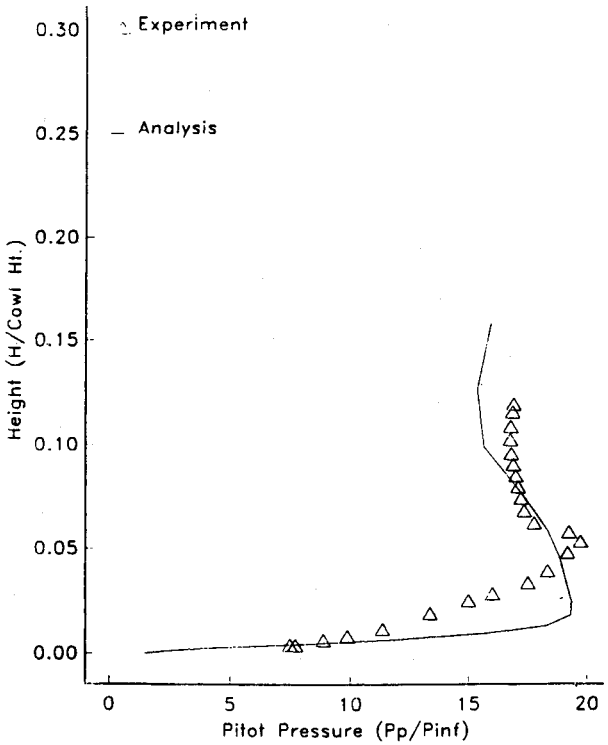

Fig. 16 Probe 2 pitot pressure profile.

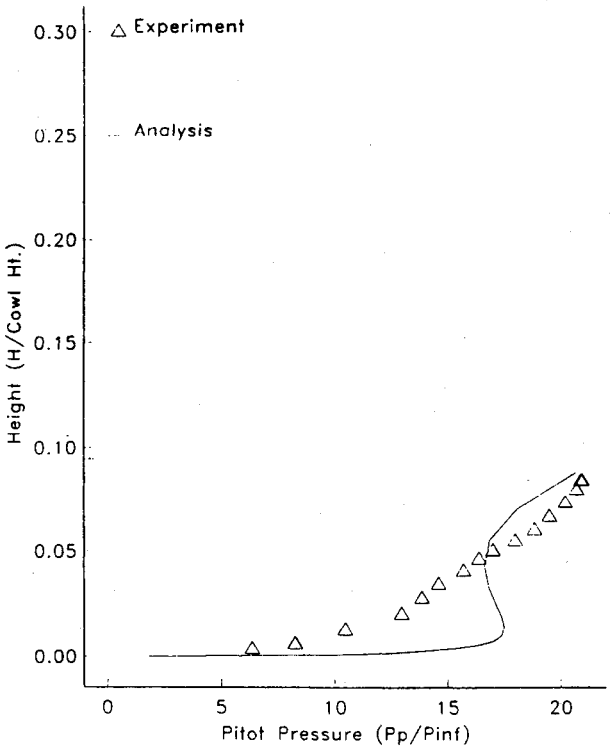

Fig. 18 Probe 9 pitot pressure profile.

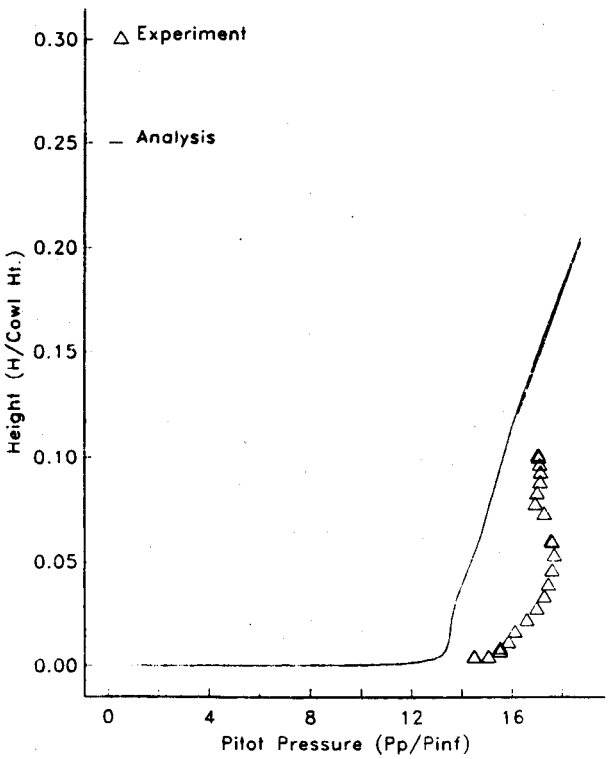

Fig. 17 Probe 5 pitot pressure profile.

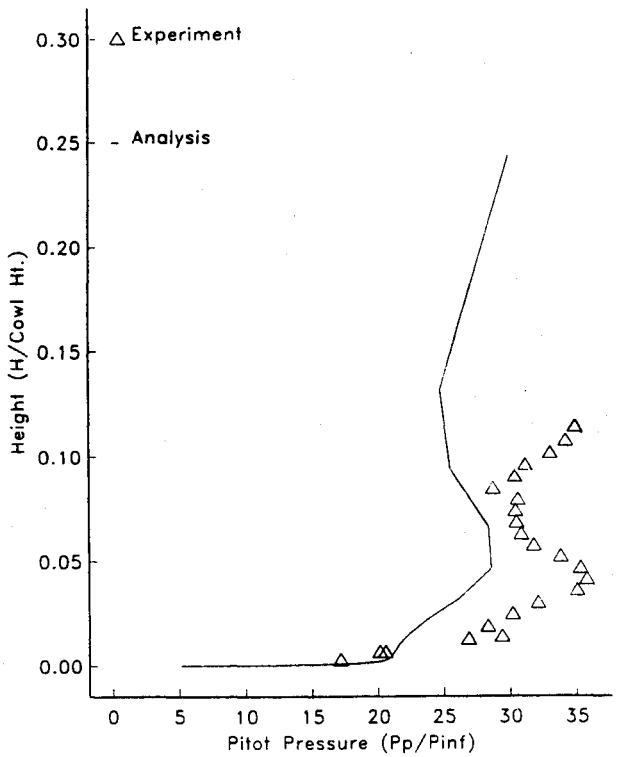

Fig. 19 Probe 10 pitot pressure profile.

computed pitot pressure contours for the two cross sections of rakes 10 and 13, as well as a third location in between. Also shown in Fig. 15b as shaded surfaces are the various bleed zones in this region. Considering the location of the rakes, the nature of the flow, and the approximations used in the turbulence model and bleed simulation, the agreement between the solution and the experimental data is reasonable. The pitot pressure profile for rake 13, shown in Fig. 14, does not show the variation of rake 10 except for a small bump very close to the corner. The pitot pressure contours for the cross section corresponding to rake 13, shown in Fig. 15, reveal that most of the vortical flow has been removed before it reached this streamwise location.

Figures 16 to 20 show pitot pressure profile comparisons for the translating probes located at different streamwise stations on the ramp as well as sidewall surfaces. Considering

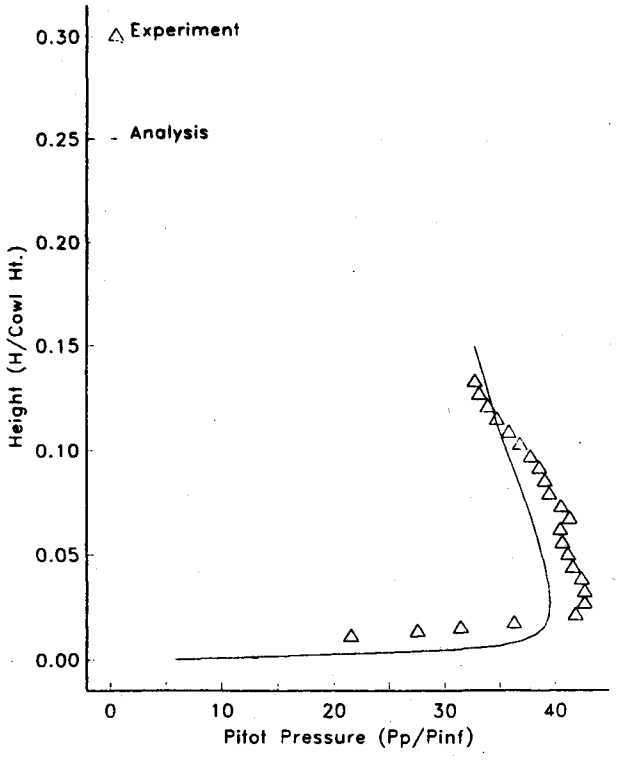

Fig. 20 Probe 11 pitot pressure profile.

that these probes are located in a very complex part of the flow, the agreement is reasonable between the solution and the experimental data for the locations away from the corner regions (probes 9 and 11). The slight disagreement in the corner regions (probes 2, 5, and 10) is, as mentioned earlier, believed to be due to the approximations used in the turbulence model and bleed simulation.

Summary

Three-dimensional viscous solution has been obtained for a Mach 5 inlet experimental configuration in order to assess the PARC3D code for hypersonic inlet applications. The flow has been computed with bleed on the inlet walls identical to that used in the experiment. The geometry of the configuration and flow conditions are identical to those of the experiment. Comparison between the solution and the experimental data indicates that the PARC3D code is reasonably capable of predicting the strong secondary flows and the three-dimensional shock/boundary-layer interaction typically present in the hypersonic inlets.

The mechanism of bleeding the undesirable vortical flow to improve the performance of the inlet has been simulated by the code. With a better understanding of the actual process that removes most of the vortical flow through the various bleed ports, the code could be used in the inlet design procedure to optimize the bleed port locations to remove the low-energy fluid efficiently and improve the inlet total pressure recovery.

Acknowledgments

This research is supported by NASA Lewis Research Center under Contract NAS3-25266 with Thomas J. Benson as monitor. The authors wish to express a deep sense of appreciation for the valuable help in generating some of the figures and many helpful discussions received from Thomas J. Benson during the course of this study. Computational analysis in this study was performed by the first author and experimental data were provided by the second author.

References

[1]Cooper, G. K., Jordan, J. L., and Phares, W. J., "Analysis Tool for Application to Ground Testing of Highly Underexpanded Nozzles," AIAA Paper 87-2015, June–July 1987.

[2]Pulliam, T. H., and Steger, J. L., "Implicit Finite-Difference Simulations of Three-Dimensional Compressible Flow," *AIAA Journal*, Vol. 18, No. 2, 1980, pp. 159–167.

[3]Pulliam, T. H., "Euler and Thin Layer Navier-Stokes Codes ARC2D, ARC3D," *Notes for Computational Fluid Dynamics User's Workshop*, Univ. of Tennessee Space Institute, Tullahoma, TN, March 12–16, 1984.

[4]Jameson, A., Schmidt, W., and Turkel, E., "Numerical Solutions of the Euler Equations by Finite Volume Method Using Runge-Kutta Time Stepping Schemes," AIAA Paper 81-1259, June 1981.

[5]Reddy, D. R., and Harloff, G. J., "Three-Dimensional Viscous Flow Computations and High Area Ratio Nozzles for Hypersonic Propulsion," *Journal of Propulsion and Power*, Vol. 7, No. 1, 1991, pp. 84–89.

[6]Reddy, D. R., Smith, G. E., Liou, M.-F., and Benson, T. J., "Three-Dimensional Viscous Analysis of a Hypersonic Inlet," AIAA Paper 89-0004, Jan. 1989.

[7]Benson, T. J., "Three-Dimensional Viscous Calculation of Flow in a Mach 5 Hypersonic Inlet," AIAA Paper 86-1461, June 1986.

[8]Kim, Y. N., Buggelin, R. C., and McDonald, H., "Numerical Analysis of Some Supersonic Viscous Flows Related to Inlet and Nozzle Systems," AIAA Paper 86-1597, June 1986.

[9]Rose, W. C., and Perkins, E. W., "Innovative Boundary Layer Control Methods in High Speed Inlet System," Final Rept., Phase I, SBIR Contract NAS3-25408, NASA Lewis Research Center, Sept. 1988.

[10]Weir, L. J., Reddy, D. R., and Rupp, G. D., "Mach 5 Inlet CFD and Experimental Results," AIAA Paper 89-2355, July 1989.

[11]Barnhart, P. J., Greber, I., and Hingst, W. R., "Glancing Shock Wave-Turbulent Boundary Layer Interaction with Boundary Layer Suction," AIAA Paper 88-0308, Jan. 1988.

[12]Gaitonde, D., and Knight, D., "The Effect of Bleed on the Flowfield Structure of the Three-Dimensional Shock Wave-Boundary Layer Interaction Generated by a Sharp Fin," AIAA Paper 88-0309, Jan. 1988.